Automated Characterization of Myocardial Scar Topological Patterns for Ventricular Tachycardia Screening

Xicheng Sheng[1†], Yang Zhang[1†], Lei Li[2], Bailiang Chen[3,4], Freddy Odille[3,4], and Xiahai Zhuang[1✉]

[1] School of Data Science, Fudan University, Shanghai, China
[2] Department of Biomedical Engineering, National University of Singapore, Singapore, Singapore
[3] CIC-IT 1433, INSERM, Université de Lorraine and CHRU Nancy, Nancy, France
[4] IADI U1254, INSERM and Université de Lorraine, Nancy, France
zxh@fudan.edu.cn
https://zmiclab.github.io/

Abstract. Ventricular tachycardia screening is crucial for early intervention and prevention of life-threatening cardiac events. Myocardial scar topology on late gadolinium enhancement (LGE) MRI offers detailed structural insights that may be closely associated with the mechanisms underlying ventricular tachycardia. However, accurate characterization presents challenges due to the substantial shape variability of myocardium, indistinct boundaries, small scar volumes, and potential issues with image quality. In this study, we present PolarNet, a novel framework for automatic scar segmentation and topological pattern characterization in polar coordinates. The framework incorporates a boundary-aware segmentation branch that explicitly models boundaries essential for scar characterization (endocardium, scar-start, scar-end, and epicardium), ensuring geometric consistency and anatomical coherence. Our method outperforms nnU-Net in both scar segmentation and topological pattern characterization. Code will be available at https://github.com/Sheng-xc/VTS_PolarNet.

Keywords: Ventricular Tachycardia · LGE MRI · Scar Topology · Polar Transformation

1 Introduction

Ventricular tachycardia (VT) is a potentially life-threatening arrhythmia characterized by rapid and irregular heartbeats originating in the ventricles [13], often associated with post-infarction myocardial scarring. Prophylactic implantable cardioverter-defibrillators (ICD) are recommended for post-infarct patients with

† These two authors contributed equally.
✉ Xiahai Zhuang is the corresponding author.

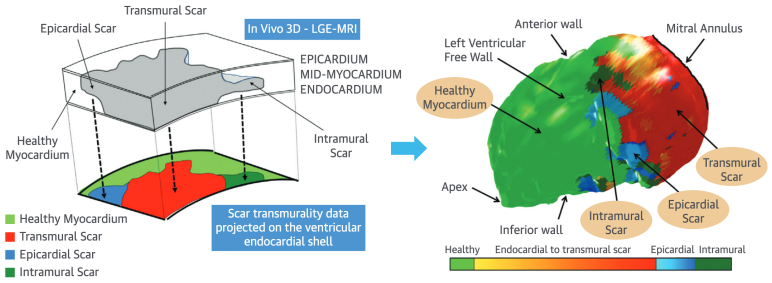

Fig. 1: Illustration of a myocardial scar with heterogeneous topological characteristics. Adapted from Fig. 1A and 1B of *JACC: Cardiovascular Imaging*, Vol. 14, de Chillou et al., "Magnetic Resonance Imaging Screening for Postinfarct Life-Threatening Ventricular Arrhythmia", pp. 2479-2481, Copyright (2021), with permission from Elsevier and the authors [1].

low left ventricular (LV) ejection fractions [14]. However, ICD implantation offers no benefit to patients without VT episodes while exposing them to potential complications, whereas LVEF-based criteria omit many at-risk individuals [17]. Therefore, more refined evaluations are needed to assess the risk of VT.

Myocardial scar tissue plays a critical role in the development of VT. Scars create heterogeneous substrates that can lead to re-entrant circuits, which are the primary mechanism of VT [3]. The topological transmurality of infarct scar, reflecting its relative position within the myocardial wall, may serve as an important marker for VT risk in postinfarct patients eligible for prophylactic ICD implantation [1]. As shown in Fig. 1, endocardial mapping of myocardial scar involves projecting scar tissue onto the endocardial shell. Each point on this projected scar surface is further classified into subtypes based on its topological relationship to the endocardial and epicardial boundaries [1].

To perform the projection, scar segmentation is essential. Numerous methodologies have been adapted for this task, ranging from traditional image processing techniques such as thresholding and region growing, to classical machine learning algorithms like SVMs and CRFs [9], and more recent deep learning architectures [10], including UNet-based models [15] and transformer-based networks [11]. Boundary quality has received limited attention, with some studies applying morphology-based [11] or signed-distance based [18] methods. Nonetheless, existing methods still struggle to accurately localize scars within the very thickness of myocardium on LGE MRI, largely due to the irregular morphology and blurred boundaries of pathological scars [12]. These inherent complexities often lead to fragmented segmentation outputs that lack anatomical consistency, making them unsuitable for applications in myocardial scar topology analysis.

Following scar segmentation, topology-based scar characterization emerged as a critical but underexplored issue. Current research in myocardial scar characterization for VT risk assessment predominantly relies on intensity-based measures of scar heterogeneity. For instance, methods based on maximum pixel signal

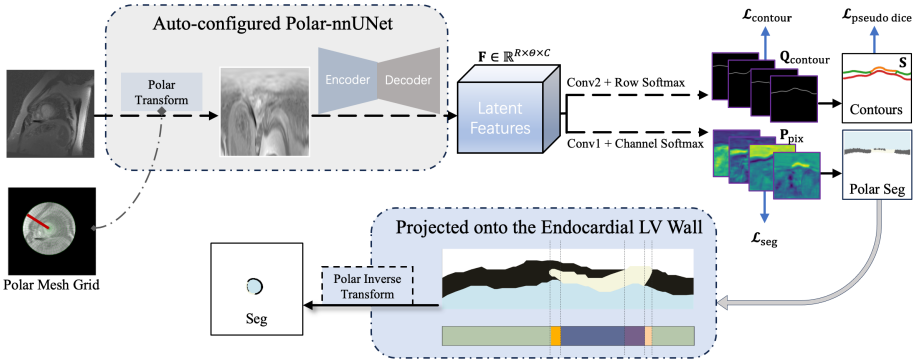

Fig. 2: The proposed framework for endocardial mapping of myocardial scar, consisting of 3 steps: 1) Anatomy-informed polar transformation, 2) Boundary-aware segmentation, 3) Projection-based subtype classification.

have been adopted to identify core and border zone for arrhythmogenic substrates on semi-automatically [4] or automatically [16] delineated myocardium and scar. Similarly, standard deviation-based thresholding methods for dense and nondense scar quantification have been performed on VGG16-initialized UNet scar segmentations [5] for prediction of major adverse cardiac events. However, these approaches do not capture the topological heterogeneity of scars, which may offer a complementary perspective for VT risk stratification.

In this work, we propose PolarNet, a novel topology-aware framework designed for boundary-sensitive myocardial scar characterization. By leveraging polar transformation, the framework enables more intuitive endocardial mapping of myocardial scar. Its dual-branch architecture integrates pixel-wise scar segmentation with explicit boundary regression, thereby enhancing anatomical coherence and segmentation accuracy. To the best of our knowledge, this is the first deep learning-based framework designed to automate the characterization of scar topological patterns, offering clinically valuable insights for VT screening.

2 Methodology

Fig. 2 presents the proposed PolarNet framework, which is designed to address the clinical demands of myocardial scar topological pattern characterization by unifying multi-class segmentation and boundary-aware regularization. The methodology is structured around three pillars: anatomy-informed polar transformation (§ 2.1), dual-branch segmentation and boundary regression (§ 2.2), and projection-based subtype classification (§ 2.3).

2.1 Anatomy-Informed Polar Transformation

The polar projection nature of endocardial mapping [2] motivates us to directly address the problem in the polar coordinate system for efficiency. To align with

the radial geometry of LV, we transform an input MRI slice $\mathbf{I} \in \mathbb{R}^{H \times W}$ into a polar representation $\mathbf{I}_{\text{polar}} \in \mathbb{R}^{R \times \Theta}$ centered at the LV centroid predicted by an anatomical segmentation model trained on public LGE MRI datasets. This transformation is implemented via grid sampling [8], using a normalized mesh grid $\mathbf{G} \in [-1, 1]^{R \times \Theta \times 2}$. Each target coordinate (r_i, θ_j) in the polar output $\mathbf{I}_{\text{polar}}$ corresponds to a sampling location in the original MRI slice $\mathbf{I}$, computed as

$$\mathbf{G}[i, j] = \left(\rho \cdot \frac{i}{R} \cos(\frac{2j\pi}{\Theta}), -\rho \cdot \frac{i}{R} \sin(\frac{2j\pi}{\Theta}) \right),$$

with $\rho \in [0, 1]$ controlling the field-of-view based on the anatomical segmentation.

2.2 Boundary-Aware Scar Segmentation

PolarNet employs a dual branch architecture inspired by structured surface segmentation for retina OCT [6]. It is built on a shared auto-configured residual encoder nnU-Net [7] backbone to extract hierarchical latent features $\mathbf{F} \in \mathbb{R}^{R \times \Theta \times C}$. These features are passed through task-specific convolutional layers to produce logits for segmentation and boundary prediction.

Segmentation Branch. The standard segmentation branch predicts pixel-wise probabilities $\mathbf{P}_{\text{pix}} \in \mathbb{R}^{R \times \Theta \times 4}$ for scar, healthy myocardium, left ventricle blood pool and background. A dice and cross-entropy loss is used for optimization:

$$\mathcal{L}_{\text{seg}} = \mathcal{L}_{\text{CE}} + \mathcal{L}_{\text{Dice}}.$$

Boundary Branch. This branch predicts four boundaries critical for topological pattern characterization of scar: endocardium ($k = 1$), scar-start ($k = 2$), scar-end ($k = 3$), and epicardium ($k = 4$). While contour regression alone cannot segment scar due to its irregular shape, it guides attention to boundaries. This branch outputs boundary probabilities $\mathbf{Q}_{\text{contour}} \in \mathbb{R}^{R \times \Theta \times 4}$ via a row-wise softmax, where $\mathbf{Q}_k[r, \theta]$ represents the probability of boundary k at angle θ occurring at radial position r. Cross-entropy loss is adopted to penalize deviations from the ground-truth boundary positions:

$$\mathcal{L}_{\text{contour}} = -\frac{1}{4\Theta} \sum_{k=1}^{4} \sum_{\theta=0}^{\Theta-1} \log \mathbf{Q}_k[\mathbf{Y}_k[\theta], \theta],$$

where $\mathbf{Y}_k[\theta]$ is the ground-truth radial position of boundary k at angle θ. As in [6], the predicted boundary position $\hat{\mathbf{S}}_k[\theta]$ is obtained using a soft-argmax operation: $\hat{\mathbf{S}}_k[\theta] = \sum_{r=0}^{R-1} r\mathbf{Q}_k[r, \theta]$. To ensure topological constraints, we apply a recursive operation: $\mathbf{S}_{k+1}[\theta] = \mathbf{S}_k[\theta] + \text{ReLU}(\hat{\mathbf{S}}_{k+1}[\theta] - \mathbf{S}_k[\theta])$, where $\mathbf{S}_k$ is the final boundary position for boundary k at angle θ. This ensures that boundaries are ordered correctly (i.e., endocardium $\leq$ scar-start $\leq$ scar-end $\leq$ epicardium).

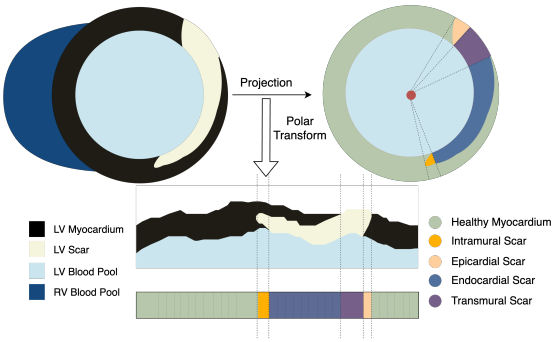

Fig. 3: Scar subtype classification via projection under polar transformation

For the endocardial boundary, epicardial boundary and scar envelope, pseudo Cartesian dice scores are computed to formulate the pseudo dice (p-dice) loss:

$$\mathcal{L}_{\text{pseudo dice}} = 2 - 2\frac{\sum_{\theta=0}^{\Theta-1} \min(\mathbf{Y}_3[\theta], \mathbf{S}_3[\theta])^2 - \max(\mathbf{Y}_2[\theta], \mathbf{S}_2[\theta])^2}{\sum_{\theta=0}^{\Theta-1} (\mathbf{Y}_3[\theta]^2 - \mathbf{Y}_2[\theta]^2) + (\mathbf{S}_3[\theta]^2 - \mathbf{S}_2[\theta]^2)} - \sum_{k=1,4} \frac{\sum_{\theta=0}^{\Theta-1} \min(\mathbf{Y}_k[\theta], \mathbf{S}_k[\theta])^2}{\sum_{\theta=0}^{\Theta-1} \mathbf{Y}_k[\theta]^2 + \mathbf{S}_k[\theta]^2}$$

further enforcing alignment between the predicted and ground truth boundaries across coordinate systems.

2.3 Projection-Based Scar Subtype Classification

The polar segmentation output is projected along the radial axis to characterize the topological distribution of myocardial scar. As illustrated in Fig. 3, this projection enables classification of each angular position θ into healthy myocardium or one of four scar subtypes—transmural, endocardial, epicardial, and intramural—based on whether the radial line intersects the scar region and whether the scar contacts the endocardium and/or epicardium. This subtype classification facilitates quantification of scar topological heterogeneity.

3 Experiments

3.1 Materials

Data Acquisition and Pre-Processing. We collected LGE MRI data within one month prior to ICD implantation from 181 post-infarct patients across five centers. All images were resampled to an unified resolution of 1.36 mm $\times$ 1.36 mm, with an intensity normalization via Z-score. The dataset was randomly devided into 126 training, 18 validation and 37 test cases.

Implementation. All experiments were conducted on a workstation equipped with an AMD EPYC 7742 64-Core Processor and an NVIDIA GeForce RTX 3090 GPU. The framework was implemented using the PyTorch library and integrated into the nnU-Net framework for efficient data processing and model training. The training process utilized stochastic gradient descent with a linear decay rate for optimization. All models were trained for 200 epochs with a batch size of 8.

Gold Standard and Evaluation. All LGE MRIs were manually labeled by an experienced cardiologist to delineate the myocardium and scar regions, which served as the ground truth for scar segmentation. The projected scar label was generated based on the manual annotations along 192 evenly spaced radii from the LV centroid, with five classes: endocardial scar, transmural scar, intramural scar, epicardial scar and healthy myocardium.

For the evaluation of scar pattern characterization, we measured performance metrics on the projected cylindrical map. Specifically, Dice, sensitivity (SEN) and specificity (SPE) were calculated for the binary classification map, where all scar subtypes were aggregated to represent the myocardial area at risk. To address the class imbalance inherent in the distribution of topological scar subtypes, we computed micro-averaged SEN and SPE, as well as the generalized Dice score (GDice)—the micro-averaged counterpart of Dice—for the multi-class classification of distinct scar subtypes.

For the evaluation of the conventional scar segmentation task, we computed standard segmentation metrics, including Dice, Hausdorff distance (HD), average symmetric surface distance (ASSD), SEN, and SPE.

3.2 Results

Results on the Task of Scar Subtype Classification and Quantification. Table 1 presents the results of the ablation study (all metrics evaluated in polar coordinates). Regarding the quantification of scar subtypes, the proposed PolarNet achieves the best GDice (0.548 ± 0.134) and SEN (0.561 ± 0.131), the latter being particularly important for screening applications in clinical practice. Compared to nnU-Net, the drop in performance observed in Polar-nnUNet may stem from the loss of fine-grained details introduced during the coordinate transformation. However, this limitation is effectively mitigated by PolarNet's dual-branch architecture, which explicitly incorporates boundary supervision. Notably, the addition of the p-Dice loss further enhances performance, contributing 1.1% and 2.2% gains in mean GDice and SEN, respectively. SPE remains consistently high ($> 94\%$) across all methods, with no statistically significant differences observed. For the overall myocardial area at risk, performance remains comparable or slightly improves after polar transformation. Addition of the boundary branch further enhances Dice and SEN. While p-Dice has limited effect on Dice/SEN, it helps recover SPE ($> 86\%$), which otherwise declines without it.

Fig. 4 visualizes the results of scar subtype classification and quantification in a representative subject. Each ring represents a short-axis slice, ordered from

Table 1: Evaluation on the task of scar subtype classification and quantification. Results shown in (mean ± standard deviation). **Bold** indicates best performance, underline indicates second best performance, asterisk (*) indicates the statistically significant difference ($p < 0.05$) given by a Wilcoxon signed-rank test between our proposed model and each comparison model.

Model	Model variants			Scar subtypes			Myocardial area at risk		
	polar	contour	p-dice	GDice	SEN	SPE	Dice	SEN	SPE
nnU-Net [7]	×	×	×	0.542* ±0.125	0.532 ±0.121*	**0.950 ±0.020**	0.793 ±0.165*	0.783 ±0.175	**0.891 ±0.084**
Polar-nnUNet	✓	×	×	0.521 ±0.144*	0.517 ±0.137*	0.944 ±0.022	0.796 ±0.169*	0.795 ±0.169	0.879 ±0.093
PolarNet (w/o $\mathcal{L}_{\text{pseudo dice}}$)	✓	✓	×	0.537 ±0.125*	0.539 ±0.117*	0.943 ±0.020	0.806 ±0.163	**0.832 ±0.152**	0.806 ±0.163
PolarNet (Proposed)	✓	✓	✓	**0.548 ±0.134**	**0.561 ±0.131**	0.942 ±0.019	**0.807 ±0.173**	0.827 ±0.164	0.860 ±0.098

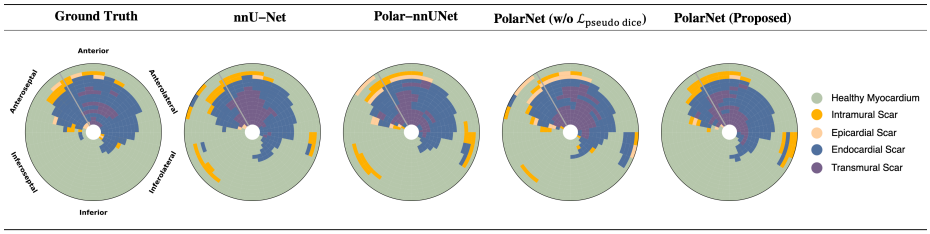

Fig. 4: Qualitative results on a typical subject for the task of scar subtype classification and quantification. Presented in a bullseye-like layout, each ring represents the classification output from a short-axis slice, with color-coded subtypes. Our proposed method (last column) yields more consistent predictions of scar presence (non-green) and improved detection of intramural scars (orange).

apical (innermost) to basal (outermost). Despite the challenge, our proposed model produces more consistent predictions of scar presence and more accurate identification of non-transmural subtypes—particularly intramural scars, which are key substrates for re-entrant VT. Notably, all methods struggle in the basal inferolateral region, likely due to image blur inherent in LGE MRI.

Results on the Task of Scar Segmentation. Our projection-based subtype classification relies on accurate scar segmentation, making segmentation quality a critical prerequisite. Table 2 summarizes the ablation study results (all metrics evaluated in Cartesian coordinates). Except for HD, the full model outperforms all ablated models, with Dice and SEN showing statistically significant gains, and ASSD improving consistently though not always significantly. The higher HD is not significant and mainly caused by outliers. Each component contributes

Table 2: Quantitative evaluation on the task of scar segmentation. Results shown in (mean ± standard deviation). **Bold** indicates best performance, underline indicates second best performance, asterisk (*) indicates the statistically significant difference ($p < 0.05$) given by a Wilcoxon signed-rank test between our proposed model and each comparison model.

Model	Metrics				
	Dice	HD(mm)	ASSD(mm)	SEN	SPE
nnU-Net [7]	0.558 ±0.148*	**13.446 ±13.034**	3.606 ±4.082*	0.552 ±0.165*	0.999 ±0.001
Polar-nnUnet	0.561 ±0.137*	13.516 ±14.826	3.387 ±4.313	0.558 ±0.150*	0.999 ±0.001
PolarNet (w/o $\mathcal{L}_{\text{pseudo dice}}$)	0.572 ±0.137*	13.469 ±15.005	3.379 ±4.990	0.582 ±0.151*	0.999 ±0.001
PolarNet (Proposed)	**0.581 ±0.139**	13.614 ±15.076	**3.340 ±3.934**	**0.599 ±0.150**	0.999 ±0.001

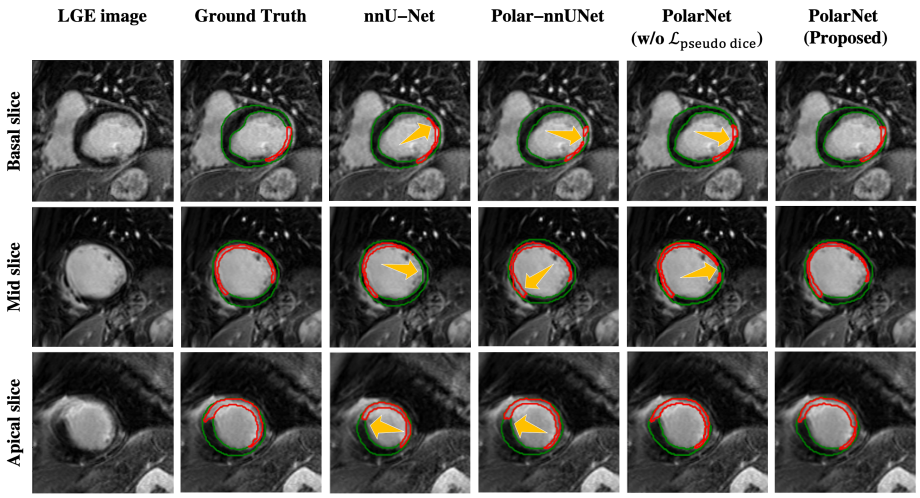

Fig. 5: Qualitative results on typical slices for the task of scar segmentation. Yellow arrows indicate outputs likely to result in implausible topological pattern characterization. The proposed method (last column; scar in red, myocardium in green) yields segmentations more suitable for scar topology analysis, showing better continuity, improved localization (rows 1–2), and sharper edge (row 3).

incrementally to the overall performance. Fig. 5 visualizes segmentation results on typical slices. Polar transformation improves the overall ability to distinguish scar regions, while the addition of the boundary branch reduces discontinuities and sharpens scar edges. These improvements help explain the superior performance observed in scar subtype classification and quantification.

4 Conclusion

Our study presents an automated framework to address the scar topological pattern characterization in LGE MRI, which is valuable in VT screening. Unlike conventional segmentation tasks, this work emphasizes the critical examination of intricate topological characteristics of myocardial scar tissue—a challenging endeavor that remains largely unexplored in existing literature. The framework's performance was quantitatively assessed using established metrics including GDice and sensitivity etc., while qualitative validation through visual analysis demonstrated alignment with clinical expert assessments. However, we recognize that this specialized clinical application may require the development of more sophisticated evaluation methodologies beyond the current conventional metrics. It should be noted that the present validation was conducted exclusively on a dataset consisting of patients with LVEF $\leq 35\%$. Future work may extend to multi-center post-infarction cohorts to improve the generalizability of our method and enable deeper analysis for enhanced clinical relevance.

Acknowledgments. This work was funded by the National Natural Science Foundation of China (grant No. 62372115) and Shanghai Municipal Education Commission-Artificial Intelligence Initiative to Promote Research Paradigm Reform and Empower Disciplinary Advancement Plan (grant No. 24KXZNA13). The authors would also like to acknowledge the support from Fédération Français de Cardiologie.

Disclosure of Interests. The authors declare no competing interests.

References

1. de Chillou, C., Voilliot, D., Amraoui, S., Duchateau, J., Marijon, E., Gandjbakhch, E., Maury, P., Sellal, J.M., Hossu, G., Cochet, H., et al.: Magnetic resonance imaging screening for postinfarct life-threatening ventricular arrhythmia. Cardiovascular Imaging **14**(12), 2479–2481 (2021)
2. Codreanu, A., Odille, F., Aliot, E., Marie, P.Y., Magnin-Poull, I., Andronache, M., Mandry, D., Djaballah, W., Régent, D., Felblinger, J., de Chillou, C.: Electroanatomic characterization of post-infarct scars. Journal of the American College of Cardiology **52**(10), 839–842 (2008)
3. Donahue, J.K., Chrispin, J., Ajijola, O.A.: Mechanism of ventricular tachycardia occurring in chronic myocardial infarction scar. Circulation Research **134**(3), 328–342 (2024)
4. Fernández-Armenta, J., Berruezo, A., Mont, L., Sitges, M., Andreu, D., Silva, E., Ortiz-Pérez, J.T., Tolosana, J.M., de Caralt, T.M., Perea, R.J., Calvo, N., Trucco, E., Borràs, R., Matas, M., Brugada, J.: Use of myocardial scar characterization to predict ventricular arrhythmia in cardiac resynchronization therapy. EP Europace **14**(11), 1578–1586 (2012)
5. Ghanbari, F., Joyce, T., Lorenzoni, V., Guaricci, A.I., Pavon, A.G., Fusini, L., Andreini, D., Rabbat, M.G., Aquaro, G.D., Abete, R., Bogaert, J., Camastra, G., Carigi, S., Carrabba, N., Casavecchia, G., Censi, S., Cicala, G., Cecco, C.N.D., Lazzari, M.D., Giovine, G.D., Roma, M.D., Focardi, M., Gaibazzi, N., Gismondi,

A., Gravina, M., Lanzillo, C., Lombardi, M., Lozano-Torres, J., Masi, A., Moro, C., Muscogiuri, G., Nese, A., Pradella, S., Sbarbati, S., Schoepf, U.J., Valentini, A., Crelier, G., Masci, P.G., Pontone, G., Kozerke, S., Schwitter, J.: AI cardiac MRI scar analysis aids prediction of major arrhythmic events in the multicenter DERIVATE registry. Radiology **307**(3), e222239 (2023)

6. He, Y., Carass, A., Liu, Y., Jedynak, B.M., Solomon, S.D., Saidha, S., Calabresi, P.A., Prince, J.L.: Structured layer surface segmentation for retina OCT using fully convolutional regression networks. Medical Image Analysis **68**, 101856 (2021)
7. Isensee, F., Jaeger, P.F., Kohl, S.A.A., Petersen, J., Maier-Hein, K.H.: nnU-Net: A self-configuring method for deep learning-based biomedical image segmentation. Nature methods **18**(2), 203–211 (2021)
8. Jaderberg, M., Simonyan, K., Zisserman, A., kavukcuoglu, k.: Spatial transformer networks. In: Advances in Neural Information Processing Systems. vol. 28, pp. 2017–2025 (2015)
9. Karim, R., Bhagirath, P., Claus, P., James Housden, R., Chen, Z., Karimaghaloo, Z., Sohn, H.M., Lara Rodríguez, L., Vera, S., Albà, X., Hennemuth, A., Peitgen, H.O., Arbel, T., Gonzàlez Ballester, M.A., Frangi, A.F., Götte, M., Razavi, R., Schaeffter, T., Rhode, K.: Evaluation of state-of-the-art segmentation algorithms for left ventricle infarct from late gadolinium enhancement MR images. Medical Image Analysis **30**, 95–107 (2016)
10. Lalande, A., Chen, Z., Pommier, T., Decourselle, T., Qayyum, A., Salomon, M., Ginhac, D., Skandarani, Y., Boucher, A., Brahim, K., de Bruijne, M., Camarasa, R., Correia, T.M., Feng, X., Girum, K.B., Hennemuth, A., Huellebrand, M., Hussain, R., Ivantsits, M., Ma, J., Meyer, C., Sharma, R., Shi, J., Tsekos, N.V., Varela, M., Wang, X., Yang, S., Zhang, H., Zhang, Y., Zhou, Y., Zhuang, X., Couturier, R., Meriaudeau, F.: Deep learning methods for automatic evaluation of delayed enhancement-MRI. The results of the EMIDEC challenge. Medical Image Analysis **79**, 102428 (2022)
11. Lecesne, E., Simon, A., Garreau, M., Barone-Rochette, G., Fouard, C.: Segmentation of cardiac infarction in delayed-enhancement MRI using probability map and Transformers-based neural networks. Computer Methods and Programs in Biomedicine **242**, 107841 (2023)
12. Li, L., Wu, F., Wang, S., Luo, X., Martín-Isla, C., Zhai, S., Zhang, J., Liu, Y., Zhang, Z., Ankenbrand, M.J., et al.: MyoPS: A benchmark of myocardial pathology segmentation combining three-sequence cardiac magnetic resonance images. Medical Image Analysis **87**, 102808 (2023)
13. Mahida, S., Sacher, F., Dubois, R., Sermesant, M., Bogun, F., Haïssaguerre, M., Jaïs, P., Cochet, H.: Cardiac imaging in patients with ventricular tachycardia. Circulation **136**(25), 2491–2507 (2017)
14. Priori, S.G., Blomström-Lundqvist, C., Mazzanti, A., Blom, N., Borggrefe, M., Camm, J., Elliott, P.M., Fitzsimons, D., Hatala, R., Hindricks, G., Kirchhof, P., Kjeldsen, K., Kuck, K.H., Hernandez-Madrid, A., Nikolaou, N., Norekvål, T.M., Spaulding, C., Van Veldhuisen, D.J.: 2015 ESC guidelines for the management of patients with ventricular arrhythmias and the prevention of sudden cardiac death: The task force for the management of patients with ventricular arrhythmias and the prevention of sudden cardiac death of the european society of cardiology (ESC)endorsed by: Association for european paediatric and congenital cardiology (AEPC). European Heart Journal **36**(41), 2793–2867 (2015)

15. Qiu, J., Li, L., Wang, S., Zhang, K., Chen, Y., Yang, S., Zhuang, X.: MyoPS-Net: Myocardial pathology segmentation with flexible combination of multi-sequence CMR images. Medical Image Analysis **84**, 102694 (2023)
16. Thomsen, A.F., Bertelsen, L., Jøns, C., Jabbari, R., Lønborg, J., Kyhl, K., Göransson, C., Nepper-Christensen, L., Atharovski, K., Ekström, K., Tilsted, H.H., Pedersen, F., Køber, L., Engstrøm, T., Vejlstrup, N., Jacobsen, P.K.: Scar border zone mass and presence of border zone channels assessed with cardiac magnetic resonance imaging are associated with ventricular arrhythmia in patients with ST-segment elevation myocardial infarction. Europace: European Pacing, Arrhythmias, and Cardiac Electrophysiology: Journal of the Working Groups on Cardiac Pacing, Arrhythmias, and Cardiac Cellular Electrophysiology of the European Society of Cardiology **25**(3), 978–988 (2023)
17. Waks, J.W., Buxton, A.E.: Risk stratification for sudden cardiac death after myocardial infarction. Annual Review of Medicine **69**(1), 147–164 (2018)
18. Zhang, J., Xie, Y., Liao, Z., Verjans, J., Xia, Y.: EfficientSeg: A simple but efficient solution to myocardial pathology segmentation challenge. In: Myocardial Pathology Segmentation Combining Multi-Sequence Cardiac Magnetic Resonance Images. vol. 12554, pp. 17–25 (2020)